Dispersion Characteristics of Open and Shielded Microstrip Lines Under a Combined Principal Axes Rotation of Electrically and Magnetically Anisotropic Substrates

Yinchao Chen and Benjamin Beker, *Member, IEEE*

Abstract— **This paper examines the dispersion properties of microstrip transmission lines whose substrate permittivity and permeability tensors are rotated simultaneously. The analysis takes into account both shielded and open structures, including both single and coupled microstrip line geometries. The spectral-domain method is utilized to formulate the dyadic impedance Green's function, and Galerkin's method is applied to find the propagation constants. Numerical studies are performed when the angular difference between the principal axes of $[\varepsilon]$ and $[\mu]$ tensors is fixed, but both are rotated from 0 to 90 degrees. The dispersion characteristics for all structures are computed over a wide frequency band that ranges from 0.1 to 100 GHz. The study indicates that propagation properties of MICs with dielectrically and magnetically anisotropic substrates (such as composites) can be changed considerably by the misalignment of material and structure coordinates systems.**

I. Introduction

In RECENT years, there has been a growing interest in the effects of principal axes rotation on the dispersion characteristics of microwave and millimeter wave integrated circuits (MICs) that use anisotropic materials as substrates. Numerous shielded structures were examined recently, including edge- and broadside-coupled lines, as well as fin-line structures [1]–[3]. In those studies, it was noted that the variation in the effective dielectric constant (ε_{eff}) is relatively small for rotation angles ranging from 0 to 90 degrees in the transverse plane, when the values of the diagonal tensor elements are not significantly different from one another. Specifically, this variation is normally about 8% or less at the lower end of the microwave frequency spectrum, but can become more prominent at millimeter-wave frequencies.

Similar observations were also made in studies dealing with open MICs. Geshiro *et al.*, presented numerical results describing propagation characteristics of open microstrips and slotlines whose permittivity tensor can be rotated in the plane of propagation [4]. This study indicates that, in general, variations in ε_{eff} due to the rotation of the material axes in the longitudinal plane are also rather small, though the slotline is more sensitive to changes in the rotation angle than the microstrip. Related work on open MICs, printed on anisotropic substrates, also includes a single microstrip line on very general anisotropic substrates [5], and coplanar waveguides on substrates characterized by Ferrites or diagonal permittivity tensors (but not both in the same layer) [6]. However, the emphasis of these two studies was on the spectral-domain formulation for substrate media with general constitutive tensor forms [5], or on the metallization thickness of the CPW structure [6], respectively.

In this paper, the spectral-domain method [7] is used to examine dispersion properties of shielded and open MICs whose principal axes of the substrate tensors are misaligned in the longitudinal plane (see Fig. 1). Moreover, the substrate material is assumed to be both dielectrically and magnetically anisotropic, which can be characteristic of composite or weakly bianisotropic media. The boundary-value problem is formulated in the Fourier-transformed domain leading to the dyadic impedance Green's function for both shielded and open microstrip transmission lines. Complete expression for the Green's function is provided so that it can be integrated into any existing, spectral-domain based, microwave CAD tools.

Galerkin's method is used to obtain a system of matrix equations whose determinant gives the desired secular equation for the propagation constant. Numerical results are computed when both the permittivity and permeability tensors are rotated simultaneously, with the angle between their principal axes in the xz-plane $\Delta\theta$ staying fixed at all times. Numerous examples of dispersion characteristics are also provided for shielded and open single or coupled microstrip line structures over a wide frequency band.

II. Theoretical Analysis

Four commonly used shielded and open microstrip transmission lines, having either one or two infinitesimally thin and perfectly conducting strips printed on their anisotropic substrates, are shown in Fig. 1. In order to analyze the effects caused by the rotation of $[\varepsilon]$ and $[\mu]$, consider the mutual misalignment angle to be the difference $\Delta\theta$ between the principal axes of the permittivity and permeability in the xz-plane. As a result, the two medium tensors will be defined

Manuscript received March 10, 1992; revised August 5, 1992.

The authors are with the Department of Electrical and Computer Engineering, University of South Carolina, Columbia, SC 29208.

IEEE Log Number 9206301.

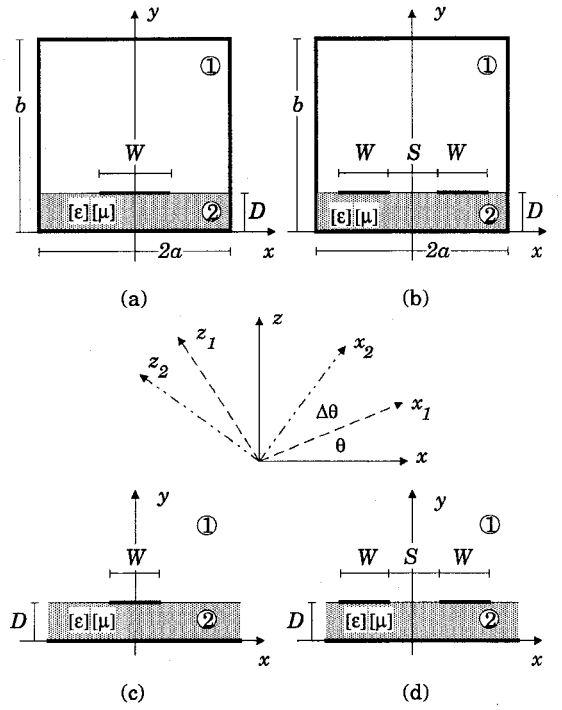

Fig. 1. Geometry of four microstrip transmission lines: (a) shielded microstrip, (b) shielded edge-coupled line, (c) open microstrip, and (d) open coupled line.

as

$$\varepsilon_0[\varepsilon_r] = \varepsilon_0 \begin{bmatrix} \varepsilon_{xx} & 0 & \varepsilon_{xz} \\ 0 & \varepsilon_{yy} & 0 \\ \varepsilon_{zx} & 0 & \varepsilon_{zz} \end{bmatrix} \tag{1a}$$

$$\mu_0[\mu_r] = \mu_0 \begin{bmatrix} \mu_{xx} & 0 & \mu_{xz} \\ 0 & \mu_{yy} & 0 \\ \mu_{zx} & 0 & \mu_{zz} \end{bmatrix}, \tag{1b}$$

where

$$\varepsilon_{xx} = \varepsilon_{x1}\cos^2\theta + \varepsilon_{z1}\sin^2\theta \tag{2a}$$

$$\varepsilon_{yy} = \varepsilon_{y1} \tag{2b}$$

$$\varepsilon_{xz} = \varepsilon_{zx} = (\varepsilon_{z1} - \varepsilon_{x1})\sin\theta\cos\theta \tag{2c}$$

$$\varepsilon_{zz} = \varepsilon_{x1}\sin^2\theta + \varepsilon_{z1}\cos^2\theta \tag{2d}$$

$$\mu_{xx} = \mu_{x2}\cos^2(\theta + \Delta\theta) + \mu_{z2}\sin^2(\theta + \Delta\theta) \tag{3a}$$

$$\mu_{yy} = \mu_{y2} \tag{3b}$$

$$\mu_{xz} = \mu_{zx} = (\mu_{z2} - \mu_{x2}) \cdot \sin(\theta + \Delta\theta)\cos(\theta + \Delta\theta) \tag{3c}$$

$$\mu_{zz} = \mu_{x2}\sin^2(\theta + \Delta\theta) + \mu_{z2}\cos^2(\theta + \Delta\theta), \tag{3d}$$

with (x_1, y_1, z_1) and (x_2, y_2, z_2) referring to the optical cordrdinate systems of $[\varepsilon]$ and $[\mu]$ of the anisotropic substrate, as shown in Fig. 1.

To formulate the MIC boundary-value problem, Fourier transforms are applied to every component of the electric and magnetic field. The transforms used for open and shielded structures are defined as:

$$\tilde{\Psi}(\alpha, y) = \int_{-\infty}^{+\infty} \Psi(x, y)e^{j\alpha x}\,dx \qquad \text{and} \tag{4a}$$

$$\tilde{\Phi}(\alpha_n, y) = \int_{-a}^{+a} \Phi(x, y)e^{j\alpha_n x}\,dx, \tag{4b}$$

respectively. Note that α_n for the enclosed structures takes on discrete integer values due to the boundary conditions at the side walls. Conversely, for open structures α is a continuous variable since no restrictions along the x direction have to be imposed. By using differential matrix operators [8], the space-domain vector wave equation for the electric field within the anisotropic substrate, when transformed to the spectral-domain, can be written as

$$[\tilde{\nabla}\times][\mu_r]^{-1}[\tilde{\nabla}\times]|\tilde{E}\rangle - k_0^2[\varepsilon_r]|\tilde{E}\rangle = |0\rangle \tag{5a}$$

or in the complete form as

$$\begin{Bmatrix} 0 & j\beta & \frac{d}{dy} \\ -j\beta & 0 & j\alpha \\ -\frac{d}{dy} & -j\alpha & 0 \end{Bmatrix} \frac{1}{\mu_d} \begin{Bmatrix} \mu_{zz} & 0 & -\mu_{xz} \\ 0 & \frac{\mu_d}{\mu_{yy}} & 0 \\ -\mu_{zx} & 0 & \mu_{xx} \end{Bmatrix} \cdot \begin{Bmatrix} 0 & j\beta & \frac{d}{dy} \\ -j\beta & 0 & j\alpha \\ -\frac{d}{dy} & -j\alpha & 0 \end{Bmatrix} \begin{Bmatrix} \tilde{E}_x \\ \tilde{E}_y \\ \tilde{E}_z \end{Bmatrix} - k_0^2 \begin{Bmatrix} \varepsilon_{xx} & 0 & \varepsilon_{xz} \\ 0 & \varepsilon_{yy} & 0 \\ \varepsilon_{zx} & 0 & \varepsilon_{zz} \end{Bmatrix} \begin{Bmatrix} \tilde{E}_x \\ \tilde{E}_y \\ \tilde{E}_z \end{Bmatrix} = \begin{Bmatrix} 0 \\ 0 \\ 0 \end{Bmatrix}, \tag{5b}$$

where $\mu_d = \mu_{xx}\mu_{zz} - \mu_{xz}\mu_{zx}$. From (5), following some algebraic manipulations, two coupled second order differential equations can be readily obtained whose matrix form is stated below

$$\begin{bmatrix} a_2\frac{d^2}{dy^2} + a_0 & b_2\frac{d^2}{dy^2} + b_0 \\ c_2\frac{d^2}{dy^2} + c_0 & d_2\frac{d^2}{dy^2} + d_0 \end{bmatrix} \begin{bmatrix} \tilde{E}_x \\ \tilde{E}_z \end{bmatrix} = \begin{bmatrix} 0 \\ 0 \end{bmatrix}, \tag{6}$$

where coefficients $a_2, a_0, b_2, b_0, c_2, c_0, d_2$, and d_0 are given in the Appendix. Physically, both x and z components of the electric field must have same variation along the y-direction, namely $e^{\gamma y}$. Moreover, in order to avoid a trivial solution to the matrix system (6), its determinant must vanish. This leads to the following fourth order characteristic equation

$$(a_2d_2 - b_2c_2)\gamma^4 + (a_2d_0 + a_0d_2 - b_2c_0 - b_0c_2)\gamma^2 + (a_0d_0 - b_0c_0) = 0, \tag{7}$$

whose roots will give the general solutions for $\tilde{E}_x(\alpha, y)$ and $\tilde{E}_z(\alpha, y)$ in terms of hyperbolic sinusoidal functions. After the boundary conditions at $y = 0$ are enforced, the explicit expressions for these two components of the electric field are given by

$$\tilde{E}_x(\alpha, y) = \left\{-\frac{b_2\gamma_a^2 + b_0}{a_2\gamma_a^2 + a_0}\right\} A_1 \sinh(\gamma_a y) + \left\{-\frac{b_2\gamma_b^2 + b_0}{a_2\gamma_b^2 + a_0}\right\} A_2 \sinh(\gamma_b y) \tag{8a}$$

$$\tilde{E}_z(\alpha, y) = A_1 \sinh(\gamma_a y) + A_2 \sinh(\gamma_b y), \tag{8b}$$

where γ_a and γ_b are the roots of (7). The remaining components of $\tilde{\vec{E}}$ and $\tilde{\vec{H}}$ fields in the anisotropic region can be obtained from Maxwell's equations directly. Specifically, $\tilde{E}_y$ can be obtained from the y component of (5b), and all components of the magnetic field can be found from

$$|\tilde{H}\rangle = \frac{j}{\omega\mu_0}[\mu_r]^{-1}[\tilde{\nabla}\times]|\tilde{E}\rangle. \tag{9}$$

The electric and magnetic fields inside the isotropic region (1) can be written as a supposition of TE^y and TM^y modes for both open and shielded MICs [9]. The y-dependence of all field components is $e^{-\gamma_1(y-D)}$ for open MICs, and $\sinh\gamma_1(y-D)$ or $\cosh\gamma_1(y-D)$ for shielded structures, respectively.

When the expressions for all tangential field components in the two regions are available, the following boundary conditions at air-strip-substrate interface can then be enforced

$$\tilde{E}_{x2}(\alpha, D) = \tilde{E}_{x1}(\alpha, D) \tag{10a}$$
$$\tilde{E}_{z2}(\alpha, D) = \tilde{E}_{z1}(\alpha, D) \tag{10b}$$
$$\tilde{H}_{x2}(\alpha, D) - \tilde{H}_{x1}(\alpha, D) = \tilde{J}_z(\alpha) \tag{10c}$$
$$\tilde{H}_{z2}(\alpha, D) - \tilde{H}_{z1}(\alpha, D) = -\tilde{J}_x(\alpha), \tag{10d}$$

where D is the thickness of the substrate. Once every boundary condition at $y = D$ has been satisfied, the dyadic impedance Green's function for both open and shielded structures is obtained and expressed in a matrix form:

$$\begin{bmatrix} \tilde{Z}_{zz}(\alpha,\beta) & \tilde{Z}_{zx}(\alpha,\beta) \\ \tilde{Z}_{xz}(\alpha,\beta) & \tilde{Z}_{xx}(\alpha,\beta) \end{bmatrix} \begin{bmatrix} \tilde{J}_z(\alpha) \\ \tilde{J}_x(\alpha) \end{bmatrix} = \begin{bmatrix} \tilde{E}_z(\alpha, D) \\ \tilde{E}_x(\alpha, D) \end{bmatrix}. \tag{11}$$

The individual elements of the Green's function are given by

$$\tilde{Z}_{zz}(\alpha,\beta) = \frac{q_{22} - q_{12}}{\Delta q} \tag{12a}$$
$$\tilde{Z}_{zx}(\alpha,\beta) = \frac{q_{12} - q_{11}}{\Delta q} \tag{12b}$$
$$\tilde{Z}_{xz}(\alpha,\beta) = \frac{B_2' q_{21} - B_1' q_{22}}{\Delta q} \tag{12c}$$
$$\tilde{Z}_{xx}(\alpha,\beta) = \frac{B_2' q_{11} - B_1' q_{12}}{\Delta q}, \tag{12d}$$

where $\Delta q = q_{11}q_{22} - q_{12}q_{21}$, with other terms given by (13) and (14a)–(14d), which appear at the bottom of the page. The remaining parameters appearing in the above equations are given by

$$\gamma_{y1} = \frac{\gamma_1}{j\omega\varepsilon_0} = \frac{\sqrt{\alpha^2 + \beta^2 - k_0^2}}{j\omega\varepsilon_0} \tag{15a}$$
$$\gamma_{z1} = \frac{\gamma_1}{j\omega\mu_0} = \frac{\sqrt{\alpha^2 + \beta^2 - k_0^2}}{j\omega\mu_0} \tag{15b}$$
$$ct_{a,b} = \coth\gamma_{a,b} D \tag{15c}$$
$$z_m = j\omega\mu_0\mu_d \cdot [\alpha^2\mu_{xx} + \beta^2\mu_{zz} + \alpha\beta(\mu_{xz} + \mu_{zx}) - k_0^2\varepsilon_{yy}\mu_d] \tag{15d}$$

with the factor

$$f(b, D) = \begin{cases} 1 \\ \coth\gamma_1(b - D) \end{cases} \tag{16}$$

used for open or shielded MICs, respectively.

Finally, once the Green's function has been derived, the Galerkin method along with Parseval's theorem can be applied to look for the propagation constants β. For all structures considered in this paper, the following basis functions were employed for single strip geometries [9]

$$J_z(x) = \frac{\cos\left[\dfrac{2(m-1)\pi x}{W}\right]}{\sqrt{1 - (2x/W)^2}} \qquad m = 1, 2, \cdots \tag{17}$$

$$J_x(x) = \frac{\sin\left[\dfrac{2m\pi x}{W}\right]}{\sqrt{1 - (2x/W)^2}} \qquad m = 1, 2, \cdots, \tag{18}$$

and their appropriate combinations were used for coupled lines.

III. Numerical Results

To verify the formulation and its numerical implementation, validation of the numerical results obtained from (11) against previously published data is provided for every structure studied in this paper. Fig. 2 shows a comparison between results for shielded ([2] and [10]) and open ([4] and [11]) MICs computed by using this method and data that is available for microstrip transmission lines with uniaxial or biaxial substrates. In addition to the validation of the formulation

$$B_{1,2}' = -\frac{b_2\gamma_{a,b}^2 + b_0}{a_2\gamma_{a,b}^2 + a_0} \tag{13}$$

$$q_{11} = \frac{\gamma_a}{z_m}(c_2 B_1' - d_2)ct_a - \frac{\beta(\beta - \alpha B_1')}{(\alpha^2+\beta^2)\gamma_{y1}} f(b, D) - \frac{\alpha\gamma_{z1}(\alpha + \beta B_1')}{(\alpha^2+\beta^2)} f(b, D) \tag{14a}$$

$$q_{12} = \frac{\gamma_b}{z_m}(c_2 B_2' - d_2)ct_b - \frac{\beta(\beta - \alpha B_2')}{(\alpha^2+\beta^2)\gamma_{y1}} f(b, D) - \frac{\alpha\gamma_{z1}(\alpha + \beta B_2')}{(\alpha^2+\beta^2)} f(b, D) \tag{14b}$$

$$q_{21} = \frac{\gamma_a}{z_m}(b_2 - a_2 B_1')ct_a + \frac{\alpha(\beta - \alpha B_1')}{(\alpha^2+\beta^2)\gamma_{y1}} f(b, D) - \frac{\beta\gamma_{z1}(\alpha + \beta B_1')}{(\alpha^2+\beta^2)} f(b, D) \tag{14c}$$

$$q_{22} = \frac{\gamma_b}{z_m}(b_2 - a_2 B_2')ct_b + \frac{\alpha(\beta - \alpha B_2')}{(\alpha^2+\beta^2)\gamma_{y1}} f(b, D) - \frac{\beta\gamma_{z1}(\alpha + \beta B_2')}{(\alpha^2+\beta^2)} f(b, D). \tag{14d}$$

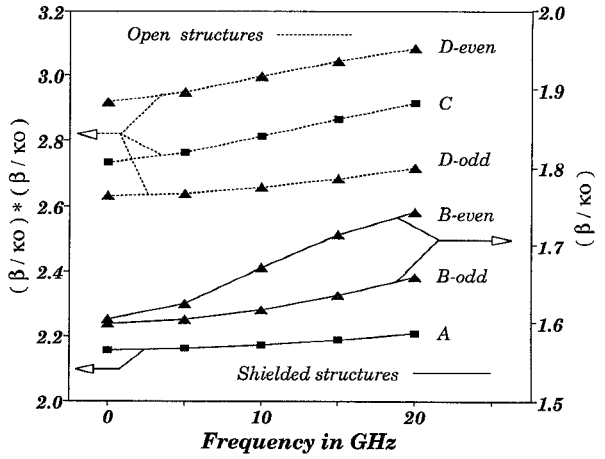

Fig. 2. Validation data for ε_{eff}. Curve A: shielded single line with $W = 2$ mm, $D = 0.5$ mm, $2a = b = 12.7$ mm, $\varepsilon_{xx} = 2.89, \varepsilon_{yy} = 2.45, \varepsilon_{zz} = 2.95$ (squares correspond to data from [10]). Curve B: shielded edge-coupled line with $W = S = D = 1.5$ mm, $2a = 8.5$ mm, $b = 4.5$ mm, $\varepsilon_{xx} = 5.12, \varepsilon_{yy} = 3.4, \varepsilon_{zz} = 5.12$ (triangles correspond to data from [2]). Curve C: open microstrip line with $W = D = 1$ mm, $\varepsilon_{xx} = 5.12, \varepsilon_{yy} = 3.4, \varepsilon_{zz} = 5.12$ (squares correspond to data from [4]). Curve D: open coupled line with $W = 1.2$ mm, $D = 0.635$ mm, $S = 0.5$ mm, $\varepsilon_{xx} = 5.12, \varepsilon_{yy} = 3.4, \varepsilon_{zz} = 5.12$ (triangles correspond to data from [11]).

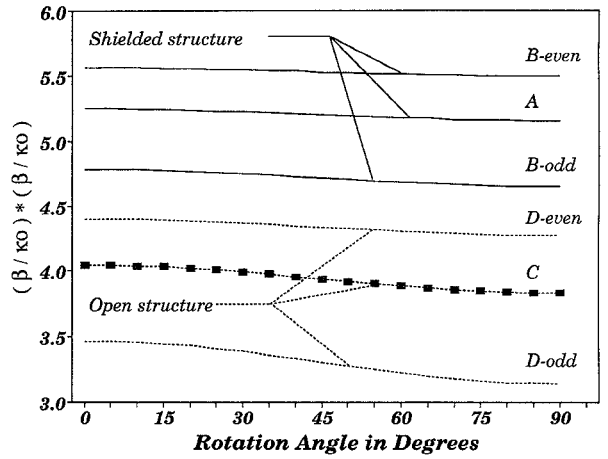

Fig. 3. ε_{eff} as a function of θ. Curve A: shielded microstrip with $f = 60$ GHz, $W = D = 0.5$ mm, $2a = b = 12.7$ mm, $\varepsilon_{x1} = 6.64, \varepsilon_{y1} = 6.24, \varepsilon_{z1} = 5.56$. Curve B: shielded edge-coupled line with same parameters as for Curve A except $S = 0.5$ mm. Curve C: open microstrip with $f = 20$ GHz, $W = D = 1$ mm, $\varepsilon_{x1} = 5.12, \varepsilon_{y1} = 5.12, \varepsilon_{z1} = 3.4$ (squares corresponding to data from [4]). Curve D: open coupled line with same parameters as Curve C except $S = 0.5$ mm.

for diagonal $[\varepsilon]$ tensors, dispersion characteristics of a single microstrip, under the rotation of its substrate permittivity tensor axes in the longitudinal plane, are also compared to those available in the literature [4], with the corresponding results displayed in Fig. 3 (case C). As can be seen from all verification studies for every structure over a wide frequency band, an excellent agreement is observed throughout.

The effects of axes rotation alone on the dispersion characteristics of all four structures, shown in Fig. 1, are displayed in Fig. 3. These results, however, only reflect the influence of the misalignment between coordinates of the waveguide

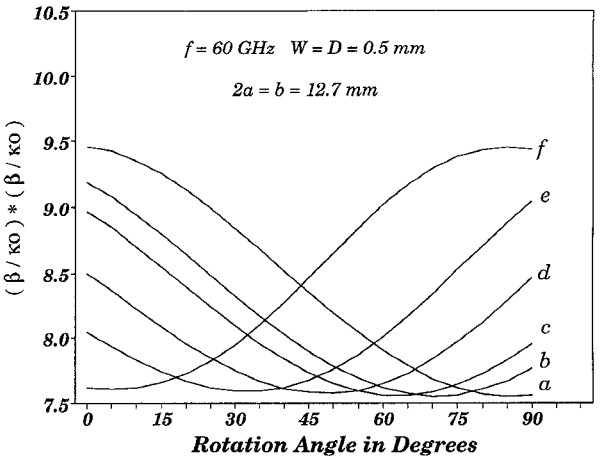

Fig. 4. $(n_{\text{eff}})^2$ as a function of θ for a shielded microstrip with $\varepsilon_{x1} = 6.64, \varepsilon_{y1} = 6.24, \varepsilon_{z1} = 5.56, \mu_{x2} = 1.86, \mu_{y2} = 1.21$, and $\mu_{z2} = 1.45$. Curves a, b, c, d, e, and f correspond to $\Delta\theta = 5$, 22, 30, 45, 60, 85 degrees.

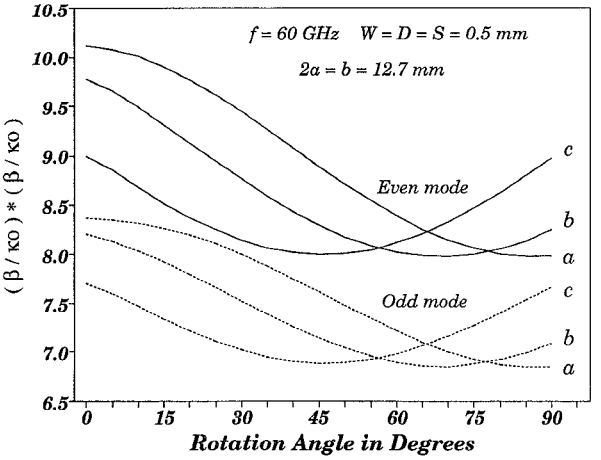

Fig. 5. $(n_{\text{eff}})^2$ as a function of θ for a shielded edge-coupled line with $\varepsilon_{x1} = 6.64, \varepsilon_{y1} = 6.24, \varepsilon_{z1} = 5.56, \mu_{x2} = 1.86, \mu_{y2} = 1.21$, and $\mu_{z2} = 1.45$. Curves a, b, and c correspond to $\Delta\theta = 3$, 22, 45 degrees.

and those of the permittivity tensor on the effective dielectric constant. Evidently, the rotation has little influence on ε_{eff} for either open or shielded MICs at several frequencies selected for computation. This behavior can be attributed to the fact that the values of the principal elements of $[\varepsilon]$ are nearly the same. The quantity, $\Delta\varepsilon_{\text{eff}}/\varepsilon_{\text{eff}}$, which gives a measure of the variation in ε_{eff}, does not surpass 8%. This, however, need not be true when the difference between the diagonal elements of the permittivity is large.

If, in addition to $[\varepsilon]$, the substrate is also magnetically anisotropic, then $(n_{\text{eff}})^2 = (\beta/k_o)^2$ becomes very sensitive within the entire range of the rotation angle. Figs. 4 through 7 illustrate specific variations in $(n_{\text{eff}})^2$ for both open and shielded MICs. In all of these numerical studies, the angle between the principal axes of $[\varepsilon]$ and $[\mu]$, namely $\Delta\theta$ is fixed, and several of its values ranging from 0 to 90 degrees are used in computations. The results indicated that now the changes in $(\beta/k_o)^2$ are no longer monotonic. Interestingly, when $\Delta\theta$

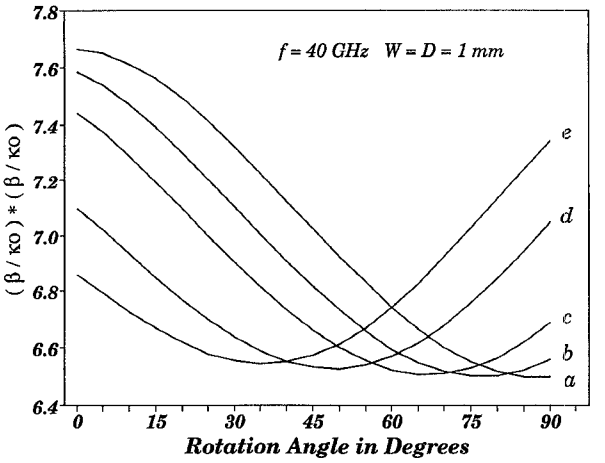

Fig. 6. $(n_{\text{eff}})^2$ as a function of θ for an open microstrip with $\varepsilon_{x1} = \varepsilon_{y1} = 5.12, \varepsilon_{z1} = 3.4, \mu_{x2} = 1.76, \mu_{y2} = 1.62$, and $\mu_{z2} = 1.48$. Curves a, b, c, d, and e correspond to $\Delta\theta = 3$, 15, 26, 45, 58 degrees.

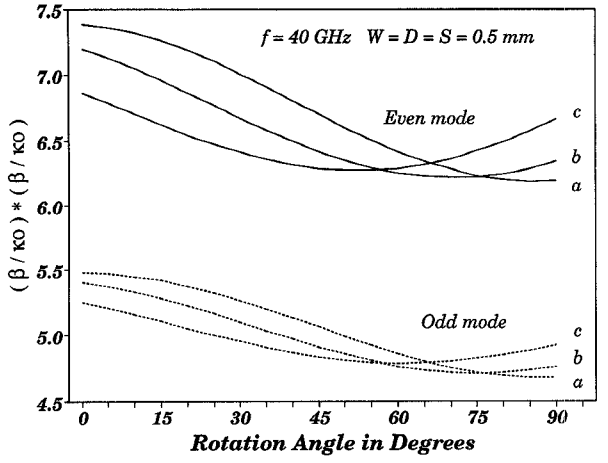

Fig. 7. $(n_{\text{eff}})^2$ as a function of θ for an open coupled line with $\varepsilon_{x1} = \varepsilon_{y1} = 5.12, \varepsilon_{z1} = 3.4, \mu_{x2} = 1.76, \mu_{y2} = 1.62$, and $\mu_{z2} = 1.48$. Curves a, b, and c correspond to $\Delta\theta = 5$, 25, 45 degrees.

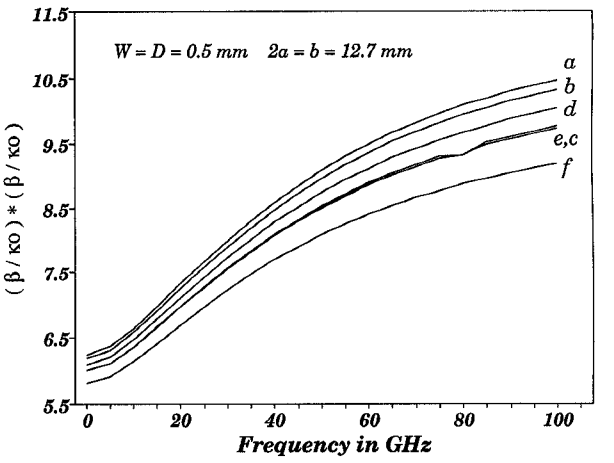

Fig. 8. Frequency dependence of $(n_{\text{eff}})^2$ for a shielded microstrip for selected $(\theta, \Delta\theta)$ values. Curves a, b, c, d, e, and f correspond to (0, 0), (10, 5), (10, 25), (16, 10), (16, 18), and (16, 33) degrees, with $\varepsilon_{x1} = 6.64, \varepsilon_{y1} = 6.24, \varepsilon_{z1} = 5.56, \mu_{x2} = 1.86, \mu_{y2} = 1.21$, and $\mu_{z2} = 1.45$.

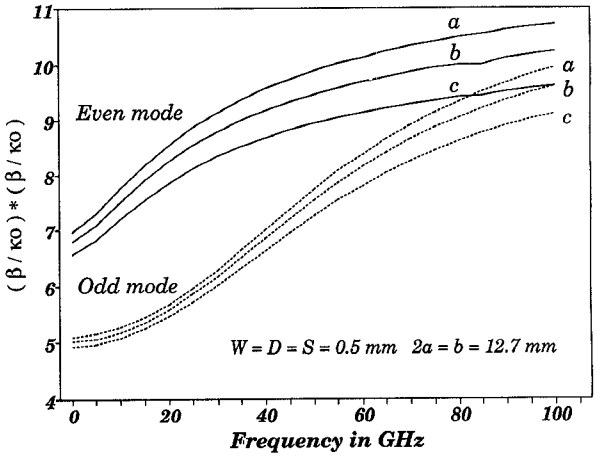

Fig. 9. Frequency dependence of $(n_{\text{eff}})^2$ for a shielded coupled line for selected $(\theta, \Delta\theta)$ values. Curves a, b, and c correspond to (0, 0), (14, 12), and (14, 28) degrees, with $\varepsilon_{x1} = 6.64, \varepsilon_{y1} = 6.24, \varepsilon_{z1} = 5.56, \mu_{x2} = 1.86$, $\mu_{y2} = 1.21$, and $\mu_{z2} = 1.45$.

is 45°, nearly all dispersion curves are practically symmetric about $\theta = 45°$, especially in Figs. 4, 5, and 6.

The effects of frequency on the propagation characteristics of open and shielded MICs are examined for several different values of θ and $\Delta\theta$. As illustrated in Figs. 8 through 11, a considerable change in $(n_{\text{eff}})^2$ can be observed as θ and $\Delta\theta$ have other values than zero. For every structure, increasing values of θ and/or $\Delta\theta$ tend to reduce the magnitude of $(n_{\text{eff}})^2$ over the entire frequency band ranging from 0.1 to 100 GHz. It is also interesting to note from Fig. 8, that it is possible to achieve nearly identical dispersion characteristics for two different sets of values of θ and $\Delta\theta$. Specifically, this is shown by curves e and c of Fig. 8 with $(\theta, \Delta\theta)$ being $(16°, 18°)$ and $(10°, 25°)$, respectively. In addition, for coupled lines, both shielded as well as open, the quantity $(\beta/k_o)^2$, for odd and even modes, approaches higher frequencies at different slopes (see Figs. 9 and 11). This trend seems to suggest that at even higher frequencies (greater than 100 GHz) both odd and even modes may reach an equiphase point.

Finally, to perform the computations for both the validation and rotation studies, IBM compatible 33 MHz, 386- and 486-based PCs were used. For both single and coupled transmission lines, shielded or open, it was found that one or two expansion functions were sufficient to achieve convergence, but two were actually used. Also, for shielded lines 250 Fourier terms were found to be adequate to account for x-dependence of the fields. Typical CPU times for either single or coupled lines ranged from 25 to 8 seconds for shielded structures, and from 46 to 15 seconds for open structures on the 386- and 486-based PCs, respectively.

IV. Conclusion

In this paper, the spectral-domain method was used to formulate and examine dispersion properties of both shielded and open MICs. In particular, effects of misalignment between the principal axes of the substrate, characterized by both $[\varepsilon]$ and $[\mu]$, and those of the structure were studied in detail.

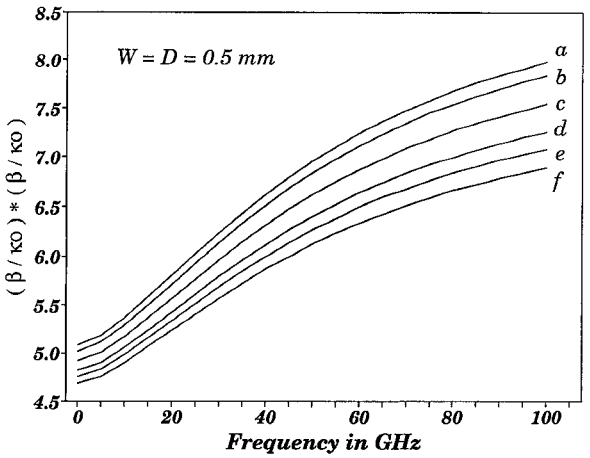

Fig. 10. Frequency dependence of $(n_{\text{eff}})^2$ for an open microstrip for selected $(\theta, \Delta\theta)$ values. Curves a, b, c, d, e, and f correspond to (0, 0), (15, 5), (15, 22), (15, 36), (15, 45), and (15, 58) degrees, with $\varepsilon_{x1} = \varepsilon_{y1} = 5.12, \varepsilon_{z1} = 3\,4, \mu_{x2} = 1.76, \mu_{y2} = 1.62$, and $\mu_{z2} = 1.48$.

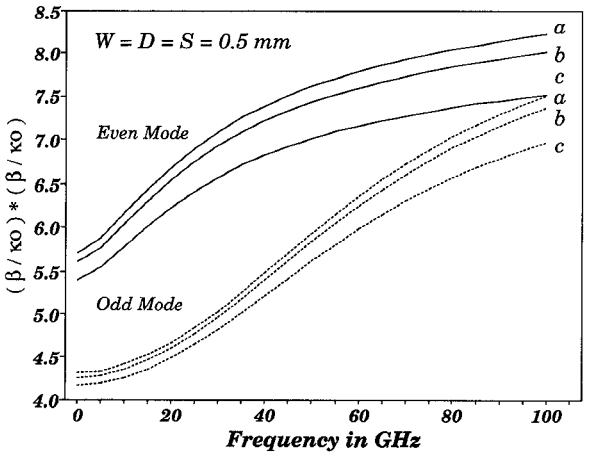

Fig. 11. Frequency dependence of $(n_{\text{eff}})^2$ for an open coupled line for selected $(\theta, \Delta\theta)$ values. Curves a, b, and c correspond to (0, 0), (15, 8), and (15, 32) degrees, with $\varepsilon_{x1} = \varepsilon_{y1} = 5.12, \varepsilon_{z1} = 3.4, \mu_{x2} = 1.76, \mu_{y2} = 1.62$, and $\mu_{z2} = 1.48$.

It was found that misalignment in both the permittivity and permeability can greatly alter the propagation properties of open and enclosed transmission lines. It was also shown that it is possible to have nearly identical dispersion curves for properly chosen values of axes rotation and the difference angles between the principal coordinate systems of $[\varepsilon]$ and $[\mu]$.

APPENDIX

The coefficients of the coupled, second order differential equations for $\tilde{E}_x(\alpha, y)$ and $\tilde{E}_z(\alpha, y)$ that appear in (6) are given by

$$a_2 = \beta^2\mu_d - k_0^2\varepsilon_{yy}\mu_{xx}\mu_d \tag{A-1a}$$

$$a_0 = \left(k_0^2\varepsilon_{xx} - \frac{\beta^2}{\mu_{yy}}\right)\mu_d G_0 \tag{A-1b}$$

$$b_2 = -\alpha\beta\mu_d - k_0^2\varepsilon_{yy}\mu_{zx}\mu_d \tag{A-2a}$$

$$b_0 = \left(\frac{\alpha\beta}{\mu_{yy}} + k_0^2\varepsilon_{xz}\right)\mu_d G_0 \tag{A-2b}$$

$$c_2 = -\alpha\beta\mu_d - k_0^2\varepsilon_{yy}\mu_{xz}\mu_d \tag{A-3a}$$

$$c_0 = \left(\frac{\alpha\beta}{\mu_{yy}} + k_0^2\varepsilon_{zx}\right)\mu_d G_0 \tag{A-3b}$$

$$d_2 = \alpha^2\mu_d - k_0^2\varepsilon_{yy}\mu_{zz}\mu_d \tag{A-4a}$$

$$d_0 = \left(k_0^2\varepsilon_{zz} - \frac{\alpha^2}{\mu_{yy}}\right)\mu_d G_0 \tag{A-4b}$$

$$G_0 = \alpha^2\mu_{xx} + \beta^2\mu_{zz} + \alpha\beta(\mu_{xz} + \mu_{zx}) - k_0^2\varepsilon_{yy}\mu_d, \tag{A-5}$$

where μ_d is the determinant of the permeability tensor.

REFERENCES

[1] S. K. Koul and B. Bhat, "Generalized analysis of microstrip-like transmission lines and coplanar strips with anisotropic substrate for MIC, electrooptic modulator, and SAW applications," *IEEE Trans. Microwave Theory Tech*, vol. MTT-31, no. 12, pp. 1051–1058, Dec. 1983.

[2] A. A. Mostafa, C. Krowne, and K. Zaki, "Numerical spectral matrix method for propagation in general layered media: application to isotropic and anisotropic substrates," *IEEE Trans. Microwave Theory Tech.*, vol. MTT-35, no. 12, pp. 1399–1407, Dec. 1987.

[3] T. Q. Ho and B. Beker, "Analysis of bilateral fin-lines on anisotropic substrates," *IEEE Trans Microwave Theory Tech.*, vol. 40, no. 2, pp. 405–409, Feb. 1992.

[4] M. Geshiro, S. Yagi, and S. Sawa, "Analysis of slotlines and microstrip lines on anisotropic substrates," *IEEE Trans. Microwave Theory Tech.*, vol. 39, no. 1, pp. 64–69, Jan. 1991.

[5] J. L. Tsalamengas, N. K. Uzunoglu, and N. G. Alexopoulos, "Propagation characteristics of a microstripline printed on a general anisotropic substrate," *IEEE Trans. Microwave Theory Tech.*, vol. MTT-33, no. 10, pp. 941–945, Oct. 1985.

[6] T. Kitazawa and T. Itoh, "Asymmetrical coplanar waveguide with finite metallization thickness containing anisotropic media," *IEEE Trans. Microwave Theory Tech.*, vol. 39, no. 8, pp. 1426–1432, Aug. 1991.

[7] T. Itoh and R. Mittra, "Spectral-domain method for calculating the dispersion characteristics of microstrip lines," *IEEE Trans. Microwave Theory Tech.*, vol. MTT-21, no. 7, pp. 496–499, July 1973.

[8] Y. Chen and B. Beker, "Analysis of single and coupled microstriplines on anisotropic substrates using differential matrix operator and spectral-domain method," vo. 41, no. 1, pp. 123–128, Jan. 1993.*IEEE Trans. Microwave Theory Tech.*

[9] T. Itoh, Ed., *Numerical Techniques for Microwave and Millimeter-wave Passive Structures*, chapter 5, New York: Wiley, 1989.

[10] T. Q. Ho and B. Beker, "Spectral-domain analysis of shielded microstrip lines on biaxially anisotropic substrates," *IEEE Trans. Microwave Theory Tech.*, vol. 39, no. 6, pp. 1017–1021, June 1991.

[11] F. Medina, M. Horno, and H. Baudrand, "Generalized spectral analysis of planar lines on layered media including uniaxial and biaxial dielectric substrates," *IEEE Trans. Microwave Theory Tech*, vol. 37, no. 3, pp. 504–511, Mar. 1989.

Yinchao Chen received the B.S. degree in physics from National Wuhan University, China, the M.S.E.E. from the University of Science and Technology of China, and Nanjing Research Institute of Electronics Technology, and the Ph.D. degree from the University of South Carolina in electrical engineering, in 1982, 1985, and 1992, respectively.

From 1982 to 1988, he was with the Microwave and Antenna Laboraotry, Nanjing Research Institute of Electronics Technology, as an engineering and research group leader working with design, research, and synthesis of microwave components and antennas. From 1988 to 1989, he was a research assistant, in the Department of Physics, University of Tennessee, Knoxville, and since 1989, he has been with the Department of Electrical and Computer Engineering, University of South Carolina, Columbia, as a research and teaching assistant.

Currently, he is a Postdoctoral Fellow in the Department, working with theory and anlysis of MICs and their discontinuities. His academic interests include microwave and millimeter-wave integrated circuits, radiation, scattering, and propagation theories and applications.

Benjamin Beker (S'83–M'88) was born in Vilnius, Lithuania, in 1959. He received the B.S.E.E., M.S.E.E., and Ph.D. degrees from the University of Illinois, Chicago, in 1982, 1984, and 1988, respectively.

From 1982 to 1988 he was a Research Assistant in the Department of Electrical Engineering and Computer Science at the University of Illinois, Chicago, working with numerically oriented scattering and radiation problems. In 1988 he joined the Department of Electrical and Computer Engineering at the University of South Carolina, Columbia, where he is now an Associate Professor.

His research interests include EM field interaction with anisotropic materials, computational methods in scattering, radiation, and guided-wave propagation in millimeter-wave integrated circuits and electronic packaging.